Progress In Electromagnetics Research B, Vol. 61, 149–168, 2014

Influence of Slots and Rotor Poles Combinations on Noise and Vibrations of Magnetic Origins in 'U'-Core Flux-Switching Permanent Magnet Machines

Guillaume Verez*, Georges Barakat, and Yacine Amara

Abstract—This paper deals with the computation of vibrations and noise of electromagnetic origin for 'U'-shaped stator core flux switching permanent magnet (FSPM) machines. The investigation concerns a family of FSPM stator/rotor configurations with 12 slots and 10, 11, 13, and 14 rotor poles. More precisely, the study focuses on the influence of different number of rotor poles on the sound power level of U-core FSPM machines. Electromagnetic forces acting on the stator frame inner surface are calculated with the Maxwell stress tensor thanks to 2-D finite element (FE) simulations. The local magnetic force density serves then as a boundary condition to the 3-D finite element vibrational simulations of the whole stator frame with housing. Finally, obtained displacements help the authors to conduct the acoustic computations using a dedicated 3-D FE analysis model. The obtained vibro-acoustic spectra help electric machines designers to make appropriate choice of stator/rotor pole combination with respect to specifications at early stages of the design process.

1. INTRODUCTION

Flux-switching permanent magnet machines are promising candidates for applications where high torque density, high speed or easy thermal management are required, as the case in the automotive industry [1]. The idea of flux-switching stems from the 1950s where it was applied on a single-phase machine [2] whereas one of the first poly-phased machines based on this principle was investigated in the late 1990s [3]. Active elements of this double salient machine are located in the stator [4]. One of its benefits is then an easy and efficient dissipation of heat generated by excitation sources [5]. Moreover, the rotor can rotate at high speed since FSPM machines combine robustness of switched reluctance machines (SRM) and high power density of permanent magnet synchronous machines (PMSM) [6].

Integer slot conventional PM machines have their dominant radial force mainly caused by the fundamental magnet field leading to a dominant vibration mode order equal to the pole number. The dominant vibration mode is linked to the lowest order of radial force harmonic. The dominant radial force of fractional slot PM machines is mainly produced by the interaction between magnet field harmonics and armature reaction field harmonics [7]. As a result, the dominant vibration mode can be as low as 1 or 2 and thus PM fractional-slot machines are generally noisier than integer slot ones. Moreover, compared to other conventional fractional-slot PM machines having same overall dimensions, FSPM machines have thinner stator teeth and reduced slot areas due to PMs placed between them [1]. FSPM machines being based on the flux concentration principle, which allows high torque density performance [5], thin stator teeth lead unfortunately to high local magnetic saturation, and to substantial magnetic stress and vibrations [4].

Received 9 October 2014, Accepted 5 November 2014, Scheduled 17 November 2014

* Corresponding author: Guillaume Verez (guillaume.verez@gmail.com).

The authors are with the Department of Electronic and Electrical Engineering, GREAH, University of Le Havre, 76057 Le Havre, France.

The optimal combination of stator and rotor pole numbers in terms of back electromotive force (EMF) and electromagnetic torque has been looked into recently [1]. It led to an overview of the most suitable winding configuration with optimal stator and rotor poles combination to achieve best electromagnetic performances. Therefore, the present study aims at characterizing the influence of such combinations on noise and vibrations. Only the influence of noise of electromagnetic origins is investigated, using finite element analysis (FEA).

The majority of publications regarding noise and vibrations concern stators which are made of a single steel sheet in the lamination plan, and thus cannot be applied to 'U'-core FSPM machines. Actually, the core being segmented leads to a completely different vibrational behavior, which depends on the way PMs and laminations are attached. Stresses located on the stator inner radius and at the interface of PMs and steel have been studied in [4]. As stresses at the interface of PMs have small amplitude compared to normal stresses at the air gap interface with the stator, they will not be modeled in this study.

The 12 slots 10 rotor poles (12s10rp) FSPM design which was first proposed in [3] has been widely studied with the same dimensions [1, 6, 8, 9]. As a result, in order to provide available basis for comparisons, it will be used. The machine is short since the ratio of the axial length over the external radius is roughly 0.5. Therefore, the use of mechanical and acoustical three-dimensional (3-D) FEA is mandatory to investigate the effect of the housing. 3-D effects at the edges are responsible for non-uniformity of stresses along the air gap's axial length but, for the sake of simplicity, a 2-D electromagnetic FEA model is assayed. FEA computations are achieved using electromagnetic and vibro-acoustic commercial software.

The paper is structured as follow. Investigated FSPM machines have their topology and dimensions presented in Section 2. The on-load air gap flux densities and electromagnetic forces calculations are explained and results are discussed in Section 3. The force is also plotted at no-load to show the impact of load on the force harmonic content. Then, the mechanical and acoustical models and computations are presented in Section 4. Details about the effect of cores laminations and frame are provided. Finally, concluding remarks are expressed.

2. TOPOLOGIES

The first three-phase FSPM machine was designed with 12 slots and PMs and 10 rotor poles (12s10rp) [3]. Many studies were performed on this machine even though no method was presenting an optimal stator and rotor pole numbers until [1]. Feasible combinations for a three-phase FSPM machines with magnets are given in (1) [1].

$$\begin{cases} N_s = 6k_1, \quad k_1 \in \mathbb{N}^* \\ N_r = N_s \pm k_2, \quad k_2 \in \mathbb{N}^* \end{cases} \tag{1}$$

N_s is the slot and magnet numbers, which must be even and N_r is the rotor pole number. Thus, for a 12-slot machine, any rotor could potentially be chosen, except $N_r = N_s$. However, N_s and N_r should be close to each other to optimize torque density [1, 10]. However, in order to minimize torque ripple, a sinusoidal back EMF is desirable [11]. In [10], authors showed that even if the single coil back EMF waveform is asymmetric, the phase back EMF is symmetrical. The winding configuration of studied topologies will be all poles wound and thus, in order to obtain balanced symmetrical back EMF waveforms in three-phase all-poles-wound FSPM machines condition (2) has to be satisfied [1]. This expression originates from the realization of a 180 electrical degrees phase shift between two coils in one phase of the machine.

$$\frac{N_s}{\mathrm{GCD}\,(N_s, N_r)} = 6k, \quad k \in \mathbb{N}^* \tag{2}$$

In this equation, GCD refers to the greatest common divisor. The difference between all-poles-wound and alternate-poles wound machine is pictured in Fig. 1 [1]. For $N_s = 12$, the only rotor poles possibilities that satisfy this relation, and that are close to 12, are $N_r \in \{10, 11, 13, 14\}$. As a result, 12s{10,11,13,14}rp configurations will be studied. Their corresponding winding connections are derived from coil-EMF vectors in electrical degrees. Electrical degrees α_e between two vectors is obtained

from mechanical degrees α_m as in (3) for conventional fractional-slot PM machines and (4) for FSPM machines [12]

$$\alpha_e = p\alpha_m \tag{3}$$

$$\alpha_e = N_r\alpha_m \tag{4}$$

Thus, in FSPM machines, the rotor pole number is equivalent to the number of pole pairs of conventional PM machines. In the present case, $\alpha_m = 30°$. Plotting two opposite sectors containing 120° (360°/3 phases), coils for one phase are obtained, as shown in Fig. 2 for investigated configurations. Coils corresponding to vectors in the opposite sector have to be connected with opposite polarity.

For every studied configuration, the stator dimensions are the same. Stator teeth cannot be too narrow otherwise they would be overly saturated and it would reduce flux linkage. However, expanding stator teeth width above an optimal value of tooth width (equal to the width of the slot openings) would lead to a reduced electromagnetic torque, for same copper losses [8]. For that reason, widths of stator teeth are taken equal to that of slot openings. Torque is also influenced by the stator inner to outer radius ratio. It was found that for the 12s10rp topology, this optimal ratio is equal to 0.6 [8]. Finally torque is also influenced by rotor poles width which should be 1.4 to 1.6 times the width of slot openings [8]. Machines parameters are chosen accordingly to previous explanations and as a result, rotor poles dimensions are equal in every combination. The only difference being the space between them. They are given in Table 1 and depicted in Fig. 3.

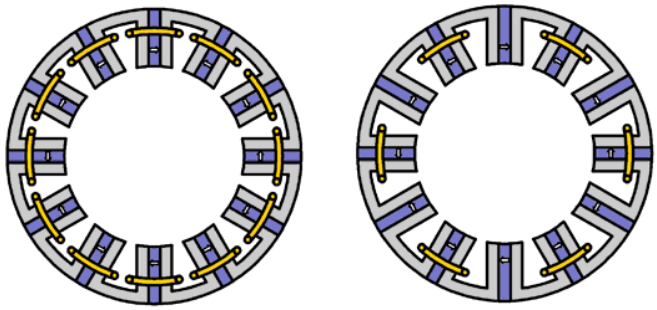

Figure 1. 12 slots FSPM machines with (a) all poles wounds and (b) alternate poles wounds [12].

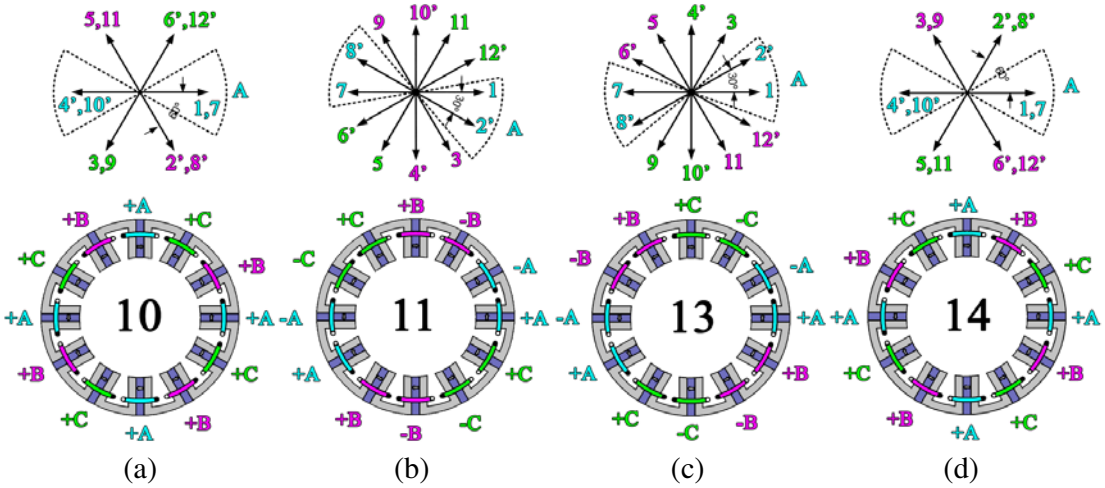

Figure 2. Winding configurations of all-poles-wound FSPM machines with 12 slots and (a) 10, (b) 11, (c) 13 and (d) 14 rotor poles.

Table 1. Machines parameters.

Symbol	Name	Value (unit)
R_{sh}	Shaft radius	10.2 (mm)
R_r	Rotor radius	20.4 (mm)
h_r	Rotor tooth height	6.6 (mm)
g	Air gap thickness	0.5 (mm)
h_s	Stator slot height	13.9 (mm)
R_{ext}	External radius	45 (mm)
θ_{unit}	Unit angle	$2\pi/N_s$ (rad)
θ_s	Slot angle	$\theta_{unit}/4$
θ_r	Base rotor tooth angle	$1.5 \times \theta_s$
L_{ax}	Core axial stack length	25 (mm)
	Rated speed	400 (rpm)
	Turns per phase	72
	Phase current	11 (A, rms)
	Slot fill factor	0.7
	Initial relative permeability of laminations	1273
	Saturation magnetization of laminations	2.15 (T)
	Remanent flux density of PMs	1.2 (T)
	Relative permeability of PMs	1.05

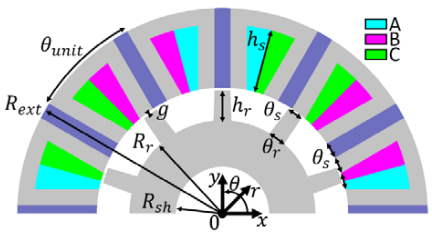

Figure 3. Cross-sectional view of half of the 12s10rp FSPM machine.

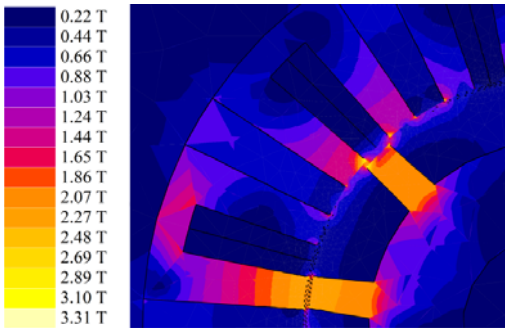

Figure 4. Flux density amplitude distribution inside the 12s10rp FSPM.

3. ELECTROMAGNETIC FORCE DENSITY COMPUTATION

3.1. Electromagnetic FEA Model

The machine is short compared to its external radius and thus 3-D edge effects should be taken into account. However, 3-D vibrational FEA computation showed that these effects are mainly responsible for second mode order longitudinal deformations that, in the present case, are excited at frequencies higher than the hearing range. In addition, edge effects do not have much influence on results in the active part of the machine. Thus, even if 3-D electromagnetic simulation is necessary to understand end-windings effects, in the case of the present study, its cost in the machine is not justified in relation with the expected precision on the vibration spectrum. As a result, electromagnetic calculations are achieved using 2-D commercial FEA software (Flux). More clearly, step-by-step simulations were made to determine the air gap flux density distribution for the rated speed on-load. The motor is assumed to

be supplied by a three-phase sine current. As in FSPM machines, the rotor pole number is equivalent to the number of pole pairs of conventional PM machines, the frequency of the phase current, f, which is proportional to the rotating speed in revolutions per minute, n_r, depends on the rotor topology as shown by (5).

$$f = \frac{N_r n_r}{60} \tag{5}$$

Width of teeth and placement of PMs and slots contribute to the high saturation level of FSPM machines [6]. Thus, saturation is taken into account in the FEA simulations by considering the nonlinear material B(H) curve of the stator and rotor laminations. PMs are NdFeB type magnets and then they are modeled by a linear B(H) curve. Saturation inside the teeth tips is shown in Fig. 4.

3.2. Locally Calculated Electromagnetic Forces

Vibrations of electromagnetic origins are due to electromagnetic pressures inside the machine. These vibrations are mainly due to normal and, to a lesser extent, tangential pressures acting at the surface of the stator inner radius. In this paper, the electromagnetic force is computed locally and it serves as a stator inner surface boundary condition for mechanical FEA. Popular methods to calculate local pressure distribution are the Maxwell stress tensor (MST) and the virtual work (VW) principle. However, each method has its advantages and drawbacks depending on the magnetic characteristics of the medium as well as on the software implementation in terms of accuracy and computation time [13].

Let $\{\overrightarrow{e_n}, \overrightarrow{e_t}\}$ be the frame of the vector space, the magnetostatic force F which is exerted the stator iron volume, V_{iron}, is expressed thanks to the MST by (6) [14].

$$\vec{F}^{(\text{MST})} = \iint_S \left[\frac{1}{\mu_0} \left(B_{n,\text{air}}^2 - \frac{1}{2} \left| \vec{B}_{\text{air}}^2 \right| \right) \overrightarrow{e_n} + \frac{1}{\mu_0} B_{n,\text{air}} B_{t,\text{air}} \overrightarrow{e_t} \right] dS \tag{6}$$

The closed surface S is the integration contour that has to lie in the air while enclosing V_{iron}. In the air gap, a closed surface limiting a volume including the stator can be constructed.

A local expressionsimilar to the MST has been derived using continuum design sensitivity analysis (CDSA) with the VW principle in [15]. Contrary to the MST, the integration takes place on the material side of the material-air interface. CDSA leads to a total force given in (7) [13].

$$\vec{F}^{(\text{VW})} = \frac{1}{2} \iint_S \left[\left(\frac{1}{\mu_0} - \frac{1}{\mu_0 \mu_r} \right) \overrightarrow{B_{\text{air}}} \cdot \overrightarrow{B_{\text{iron}}} \right] \overrightarrow{e_n} dS + \frac{1}{2} \iiint_{V_{\text{iron}}} \nabla \frac{1}{\mu_0 \mu_r} \overrightarrow{B_{\text{iron}}} \cdot \overrightarrow{B_{\text{iron}}} d\text{V} \tag{7}$$

The volume term disappear in the case of a linear material or can be ignored in the case of a nonlinear material [16]. Global stress has been shown to be equivalent for (6) and (7) in a 'C'-core actuator structure depicted in [15]. Locally, for a non-linear material not fully saturated, (6) and (7) yield similar force distribution since permeability is high and the nonlinearity of the material smoothes corner singularities [16]. As a result, the MST can be employed to accurately derive the local electromagnetic force density at the surface of the stator inner radius, especially for comparison purposes between different machine geometries.

3.3. Results

Simulations are done on-load, for nominal conditions (maximum torque obtained by choosing the adequate phase shifting between EMFs and armature currents). Mean electromagnetic torque values are given in Table 2 and are close to values obtained by FE simulations in [1]. Average torque increases with rotor pole number and 12s{13,14}rp configurations exhibit similar mean torques. The normal and tangential components of the air gap flux density are shown in Fig. 5 for every investigated combination. Their spatial harmonic content is also shown. The high values of the normal components of the air gap flux density are due to the magnetic flux concentration in the stator and rotor teeth. Tangential components are particularly high, reaching for some angular positions, their normal counterparts. Harmonic contents are plotted considering that the fundamental harmonic has a period of 360 mechanical degrees. As a consequence, configurations 12s{10,14}rp having GCD $(N_s, N_r) = 2$ show only even harmonics. One can observe the increase of the 6th and 18th harmonics with the increase of rotor pole number.

Table 2. Mean electromagnetic torque of 12-stator slots FSPM machines.

N_r	Mean torque (N · m)
10	2.97
11	3.12
13	3.53
14	3.55

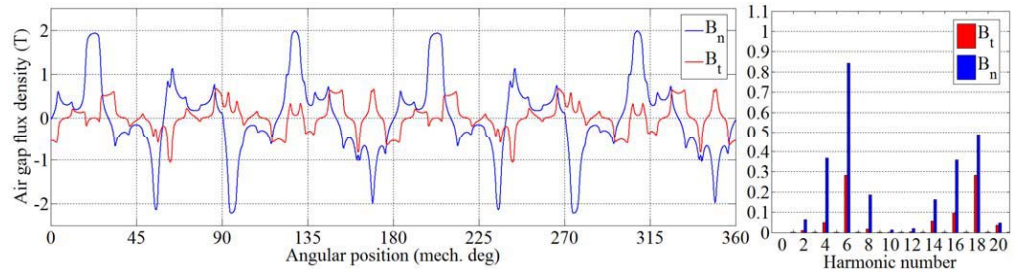

(a) 12s10rp

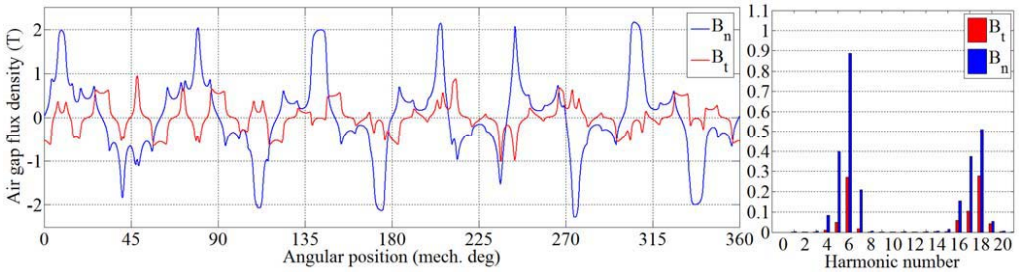

(b) 12s11rp

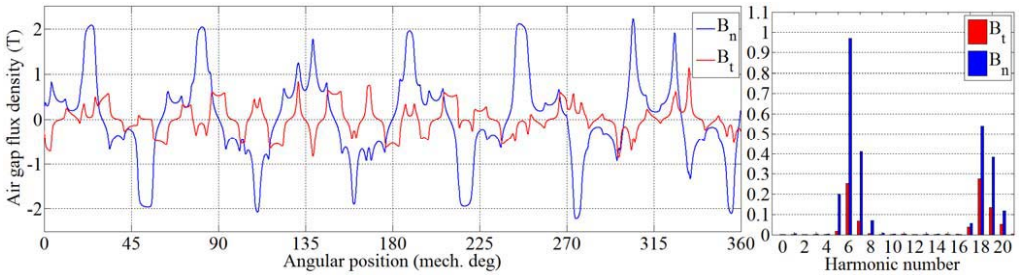

(c) 12s13rp

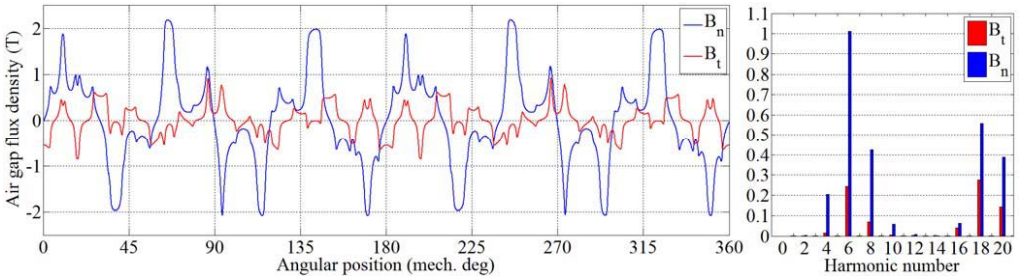

(d) 12s14rp

Figure 5. Comparison of FE predicted air gap flux density components in 12s{10,11,13,14}rp loaded FSPM machines.

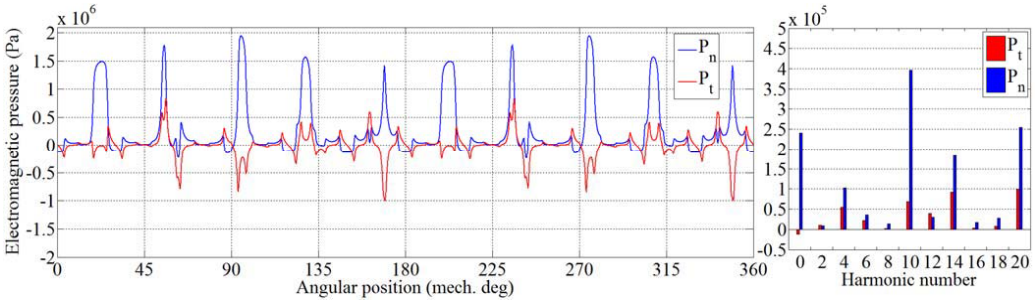

(a) 12s10rp

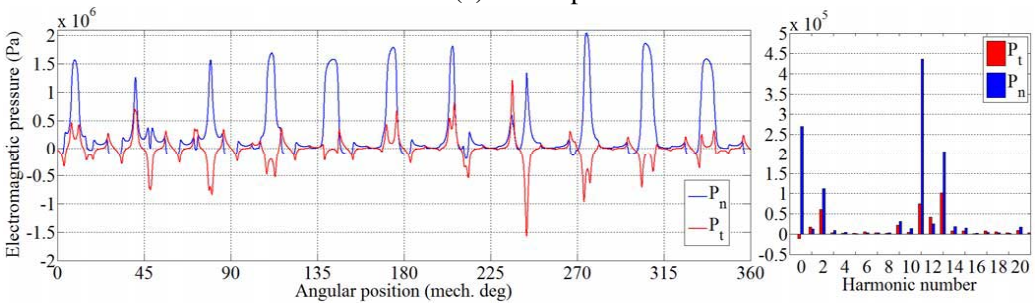

(b) 12s11rp

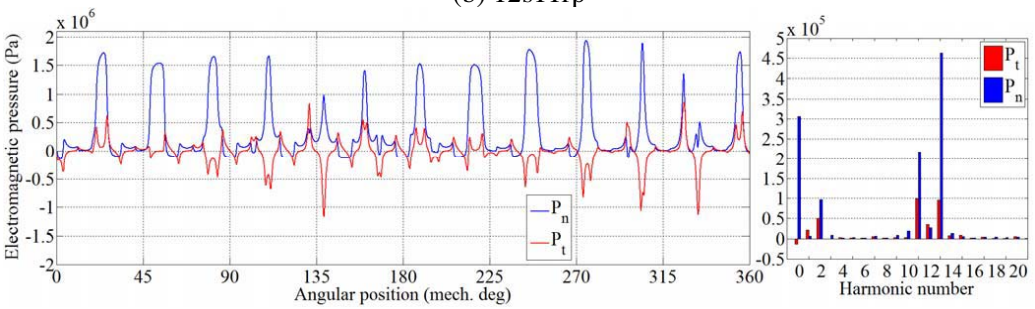

(c) 12s13rp

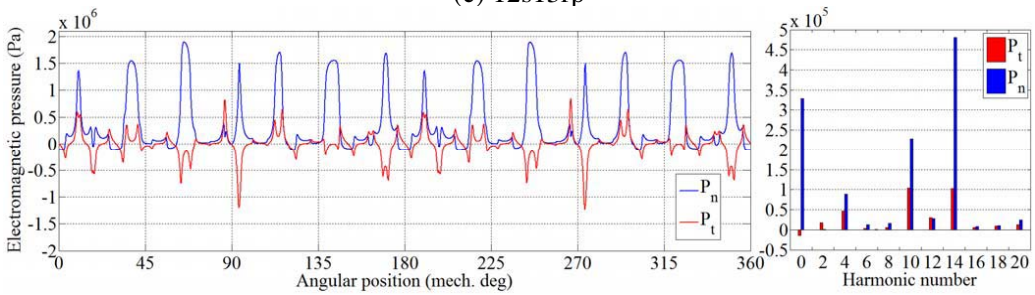

(d) 12s14rp

Figure 6. Comparison of FE predicted electromagnetic force density components in 12s{10,11,13,14}rp loaded FSPM machines.

For each combination, the normal and tangential components of the electromagnetic pressure are plotted in Fig. 6. The highest amplitudes harmonics are the $kN_r,\ k \in \mathbb{N}$ harmonic numbers. The mean amplitude value increases almost linearly with the number of rotor poles. The harmonic of rank 1 is responsible for unbalanced magnetic force since it tends to misalign the stator from the axis of rotation. This harmonic is excited in 12s11rp and 12s13rp cases. Finally, as one can expect, the harmonic of rank N_r is the more energetic and its amplitude increases with the rotor pole number.

As expected, the tangential component of the force is globally much lower than the normal component.For the sake of simplicity the tangential component was not considered in this study.

4. MECHANICAL AND ACOUSTICAL MODELS

4.1. Simplifications

Precise determination of natural frequencies is of importance in order to obtain the accurate vibration behavior of the machine. However, some structural details can be high computation time consuming and bring few accuracy to the overall results. Some simplifications listed below allow reducing FEM processing duration.

The vibro-acoustic analysis is restricted to the stator. Indeed, even if the rotor is subject to similar air gap magnetic forces than the stator it acoustically radiates less due to its structural confinement. Usually, the rotor can be neglected as an electromagnetic noise source [17]. It has been measured that the rotor's contribution is only quantifiable for low frequencies and the corresponding vibrational modes can be simply distinguished from those generated by the stator in the cylindrical frame [18]. As a result, if only the modes of the machine due to the frame and the stator are of interest, simulations can be done without rotor. The present study was conducted for an important number of structures and its main goal is to determine the major tendencies in terms of noise emission. Simulations were then done with the FEM, acknowledging that FEM provides sufficiently accurate results, with, for example, reported difference from 1 to 10% on natural frequencies [19].

Stator temperature has an influence on natural frequencies. Indeed, the latter decrease when temperature increases and for circumferential modes, differences up to 8% have been encountered between frequencies measured at room temperature and those measured at nominal operating temperature [20]. This influence is difficult to model and quantify because it impacts conductors insulation and the other materials behavior. In general, for metals, Young's modulus decreases when temperature rises whereas Poisson's ratio increases. In this paper, influence of temperature is not considered and FEM computations are achieved at constant room temperature.

Conductor insulation is taken into account by modifying Young's modulus of coils, which are considered mechanically isotropic. Coil bonding put aside, coil insulation such as impregnation and heating reduce stator damping. Thus, amplitudes of vibrations at resonance frequency are larger. It is therefore a drawback in terms of noise cancelation but also a benefit since impregnation suppresses a lot of parasitic resonant frequencies in the stator, leading to a much clearer vibration or noise spectrum [21].

Structural complexity of a real machine makes it tedious to model with FEM down to the very last detail. Usually, elements which have complex geometric shapes are approximated with simple shapes such as cylinders, beams, etc.. Unfortunately, materials can never be perfectly taken into account and mechanical coupling between bearing shields and the frame is difficult. Thus, natural frequencies calculated with the FEM are in close agreements with experimental tests but errors from 3% [22] to 10% [18] may occur between the two, depending on the amount of modeled details.

4.2. Influence of the Frame

Frame manufacturing having evolved throughout the decades, observations of some authors have to be put in their context. However, conditionally, some remarks can be approved. When the frame is weakly mechanically coupled to the stator, i.e., when it only wraps the stator [23], it has poor influence on natural frequencies values [21, 24]. The majority of small motors have their stator core simply pressed into the frame [25]. For large machines, amplitudes of vibrations are lower when the frame is present than when there is no frame [21]. A confirmation in case of a weak coupling is presented in [21] where the aluminum frame weights 7% of the total stator mass, its Young's modulus being smaller than the stator one and its axial length almost equal to the core stack length. However, for a frame made of steel which has a slightly higher isotropic Young's modulus than one of the stator core and higher mass density, as in [19], the frame has to be taken into account. In addition, even for small machines the frame may be much longer than the core, resulting in a strongly modified vibration behavior [19]. More specifically, the longer the frame in comparison to the core, the lower are natural frequencies of the entire machine [25].

In many machines, an air or liquid cooling system is featured. Air ducts can be installed on the stator external area whereas water ducts can be machined on the frame external area [26]. Compared to basic cylindrical shapes, these modifications change the vibro-acoustic behavior of the machine since

mass and stiffness are changed [18]. When the stator is notched, a loss of symmetry may appear if notches are not placed at regular intervals around the stator. It results in a difference between symmetric and antisymmetric modes. Thus, a single notch can reduce the antisymmetric mode by 4% compared to the symmetric one [27]. As cooling changes from a machine to another and that the studied machine is small, it is not considered in the present study.

In the FEM model, stator laminations are considered to be simply pressed into the frame [19]. Moreover, a real machine is fixed to a support, which alters boundary conditions of the structure. However, if insulators, having natural frequencies much lower than those of interest, are placed under the machine, it can be modeled without support [18]. The support can be modeled by the boundary conditions choice on the bearing shields. Bearing shields are modeled as plates with simply supported conditions.

4.3. Effect of Stator Core Laminations

The stator core is laminated in order to reduce eddy current losses [28]. In most electrical machines, the axis of rotation is normal to the plane of steel sheets [29]. Mechanical vibrations can be considered as fluctuations between potential energy and kinetic energy in a structure, as related by the Lagrange equations of the second kind. A continuous elasticity is a necessary condition to this energy variation. Some authors have ventured to consider the laminated structure as a single solid structure for calculating natural frequencies of a stator [17, 21]. For a stator core, laminations cut the elastic connection between each sheet and make impossible elastic forces transfer between them [28]. The core's vibration behavior is strongly impacted by elasticity parameters of the stack of steel sheets [30]. Moreover, when several sheets are pressed by tightening in order to make a single laminated cylinder, boundary conditions of each sheet are not the one of an isolated simply supported sheet [28].

Stator core laminations reduce the resistance of a solid equivalent. The stack is then significantly less stiff and thus more flexible [29]. As a result, amplitudes of vibrations of a laminated stator are more damped [31] and, in particular, for low mode numbers [23]. Due to this damping, longitudinal modes do not exhibit distinct peaks on the vibration spectrum unlike a solid and homogeneous core [27]. It thus leads some authors to conclude that a laminated core suppresses longitudinal modes equal to 1 [24, 27]. Damping factors obtained for solid stators decrease when frequency increase, which shows predominance of damping due to friction [31]. It has been observed in the case of a stator composed of a laminated core with bearing shields that damping factors do not show direct relation with natural frequencies. It suggests the presence of non-linear damping effects that usually occur in composite structures, made of several different materials. Values of damping factors for this structure are approximately 10 to 100 times those of a solid and homogeneous equivalent stator core [31]. It has to be noted that the vibration amplitude reduction due to damping depends on the number and thickness of steel sheets and on the type of mode [28].

The anisotropic nature of laminated cores, i.e., directionally dependent, is in general considered as orthotropy, i.e., dependency over two main perpendicular components. In linear elasticity, the elasticity stiffness tensor, issued from the general Hooke's law, has 36 components. In an isotropic case, this stiffness tensor has only 2 independent parameters among 36. They are the Young's modulus and the Poisson's ratio of the entire structure. However, in case of anisotropy, these two array parameters depend on direction and there are 21 independent scalar parameters. For orthotropy, 9 independent parameters have to be ascertained. Let E, G and ν respectively be the Young's modulus, shear modulus and Poisson's ratio. The 9 parameters in the frame of the vector space $\{x, y, z\}$ are: E_x, E_y, E_z, G_{xy}, G_{xz}, G_{yz}, ν_{xy}, ν_{xz} and ν_{yz}. They entirely depend on the considered machine since materials and lengths change from a manufacturer to the other. Thus, each author suggests experimental values which are input data to FEM models. Electrical steel allows reducing energy losses and increasing magnetic flux. For a single laminated sheet, values of the Young's modulus in the $\{x, y\}$ plane can vary from 175 GPa to 220 GPa [32].

In order to represent laminated stator cores in this study, steel with orthotropic behavior is considered [18]. The ratio of the stress over the strain along the longitudinal axis, E_z, and ratios of shear stress to the shear strains in the $\{x, z\}$ and $\{y, z\}$ planes, G_{xz} and G_{yz}, are significantly lower than equivalent moduli of solid and homogeneous materials. Thus, E_z, G_{xz} and G_{yz} do not exceed 2%

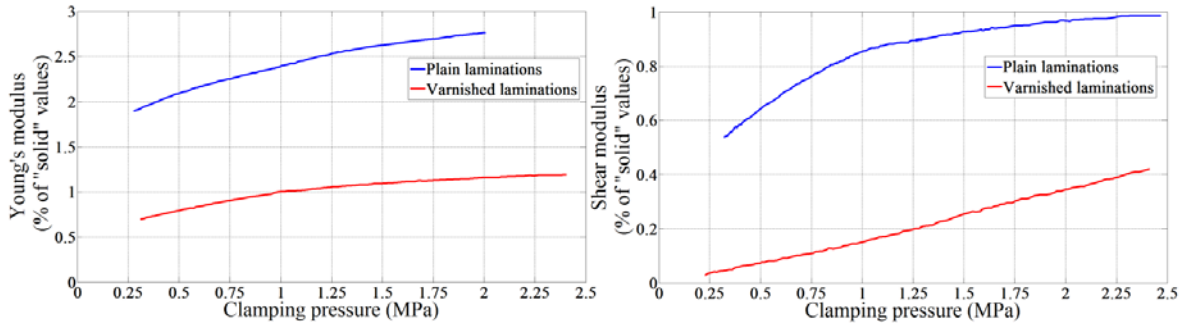

Figure 7. Percentage decrease of (a) Young's modulus and (b) shear modulus in the $\{x, z\}$ and $\{y, z\}$ planes for plain and varnished laminations compared to their solid and homogeneous solid equivalent [29].

of isotropic values. However, values of damping factors linked to normal and shear deformations are commonly 1.5% to 10%, which is significantly higher than isotropic steel [29].

The Young's modulus values, in the $\{x, y\}$ plane or in the axial direction, vary from an author to another because they are experimental values and are commensurate with a particular machine. For $E_x = E_y = 136\,\text{GPa}$, E_z has been measured to be 2.7 GPa, which is 2% of the Young's modulus value in the radial plane [18]. These results depend on sheets thickness and for example, for 0.65 mm thickness, E_z has been measured to be 0.8 GPa for a more frequently met value of $E_x = E_y = 200\,\text{GPa}$, leading to a value of E_z being 0.4% of E_x instead of 2% [29]. Although, elasticity moduli depend on clamping pressure and sheet treatments. As a result, Delvesgave a Young's modulus in the axial direction of 1.8 GPa, as quoted in [28], which is 0.9% of the value in the radial plane. For $E_x = E_y = 205\,\text{GPa}$, E_z has also been measured at 1.5 GPa which is 0.7% [33]. Subsequently, the Young's modulus in the axial direction is in the order of 0.4% to 2% to the ones found in radial directions. This extent is presented in Fig. 7(a) for 0.65 mm thick sheets where the percentage decrease of longitudinal Young's moduli of plain and varnished laminations is plotted versus their homogeneous solid equivalent [29].

For an isotropic steel material, the shear modulus, G, is usually around 80 GPa since $G = E/2\,(1+\nu)$ [34]. For a laminated material, its value is slightly lower in the $\{x, y\}$ radial plane where it has been measured at 79.3 GPa in [29], 55 GPa in [27] and 25 GPa in [33]. In the $\{x, z\}$ and $\{y, z\}$ planes, shear moduli are also reduced and measured up to 2% of aforementioned values of G_{xy}. Fig. 7(b) illustrates the shear modulus percentage decrease for plain and varnished laminations compared to a homogeneous solid equivalent [29]. A percentage value of 0.4% is used in [30], and [33] takes a value of 6% compared to a solid equivalent. In orthotropic materials, the Poisson's ratio is directional and varies with orientation of each sheet. Moreover, it is slightly higher than its solid equivalent [35]. Poisson's ratio in the $\{x, z\}$ and $\{y, z\}$ planes are also impacted by laminations. The elasticity stiffness tensor, which is symmetric, has to be positive definite so that the strain energy density can also be, according to Hooke's law [36]. However, Sylvester's criterion states that for a real symmetrical matrix to be positive definite, it is necessary and sufficient that the n (the matrix size) leading principal minors are positive [37]. Minors are determinants of its smaller square matrices. Its third minor, which satisfies this inequality, can be simplified according to (8) in the orthotropic case [35].

$$1 > \nu_{xy}^2 \frac{E_y}{E_x} + \nu_{yz}^2 \frac{E_z}{E_y} + \nu_{xz}^2 \frac{E_z}{E_x} + 2\nu_{xy}\nu_{yz}\nu_{xz} \frac{E_z}{E_x} \tag{8}$$

For electrical machines, $E_x = E_y$ and E_z measures up to 2% of E_x. As a result, Poisson's ratios in the $\{x, z\}$ and $\{y, z\}$ planes can be equal to 4 when ν_{xy} is set to 0.3. In [19, 27, 38] et al., Poisson's ratios are equal to 0.3 in every directions whereas in [33], $\nu_{xz} = \nu_{yz} = 0.03$. However, Poisson's ratio has little effect on natural frequencies [38] and thus, for major Poisson's ratio, a value of 0.3 in each direction is considered. The difference between major and minor coefficients is expressed in (9) for an orthotropic case [36]. ν_{ij} corresponds to a contraction in direction j when in direction i, an extension is applied. As a result, the minor coefficient can be at least $1/2\% = 50$ times smaller than the major

coefficient.

$$\nu_{ij} = \nu_{ji}\frac{E_j}{E_i} \tag{9}$$

From these remarks, it is clear that the vibration behavior of a stator having a laminated core is different from a stator with a core made of a single homogeneous thick cylinder [28]. Since amplitudes of vibrations are damped due to laminations, it is beneficial from a vibro-acoustic perspective in electrical machines [23]. However, since each machine has its own physical particularities, models based on the FEM cannot precisely render a machine vibration behavior without updating aforesaid orthotropic parameters.

4.4. Models

A deterministic approach is utilized in order to ascertain noise radiated by the machine. It is opposed to statistical energy analysis [39]. A mechanical FEM model has been created to describe a machine's vibration behavior and an acoustical FEM model to ascertain noise generation. FEM is in general limited to low frequencies (under 5 kHz) since the number of elements required by the model increase by a factor of 8 (in 3-D) when the frequency of interest is doubled [18]. Indeed, the base number of acoustic elements is generally high. As an example, for an acoustic sphere spawning only one sine period of sound pressure on its radius and with 50 tetrahedral elements on this radius, the total number of acoustic elements is already 100 000. However, for small machines and if calculation time is not of prime interest, it is possible to obtain good results on the entire hearing range. Moreover, the volume of air surrounding the machine that has to be modeled can be reduced in order to keep a roughly constant number of elements since their size decreases. Chosen mechanical parameters are given in Table 3.

Table 3. Physical parameters of the stator.

Parameters	Laminations	Windings	Magnets	Frame
Young's modulus in the x direction: E_x (GPa)	200	9.4	160	71
Young's modulus in the y direction: E_y (GPa)	200	9.4	160	71
Young's modulus in the z direction: E_z (GPa)	0.8	9.4	160	71
Shear modulus in the $\{x, y\}$ plane: G_{xy} (GPa)	79.3	3.5	64.5	26.7
Shear modulus in the $\{x, z\}$ plane: G_{xz} (GPa)	0.3	3.5	64.5	26.7
Shear modulus in the $\{y, z\}$ plane: G_{yz} (GPa)	0.3	3.5	64.5	26.7
Poisson's ratio in the $\{x, y\}$ plane: ν_{xy}	0.3	0.35	0.24	0.33
Poisson's ratio in the $\{x, z\}$ plane: ν_{xz}	0.0012	0.35	0.24	0.33
Poisson's ratio in the $\{y, z\}$ plane: ν_{yz}	0.0012	0.35	0.24	0.33
Mass density: ρ ($\mathrm{kg \cdot m^{-3}}$)	7700	8890	7500	2700

The frame is considered as a hollow cylinder, clamped at each ends. Several boundary conditions can be used at cylinders ends and the most encountered in case of stator or frame considers same conditions for both ends. In case of a frame, bearing shields can be thick and a clamped condition is considered [19]. As a result, displacements in the three space directions are prevented at the ends of the cylinder. In order to not constrict the machine in a bulky frame, its thickness is considered to be 1 mm. Increasing frame thickness increases natural frequencies of pure circumferential modes. In the present case, compared to a machine without frame, a thickness of 1 mm increases the frequency of the second circumferential mode by 24%, and 3 mm by 116%. Moreover, the frame is considered to be 5 mm longer at each extremities of the stack length to put the end windings. As a result, the frame weights 6.1% of the total stator mass and is 1.4 times longer. The frame cannot be neglected. The end windings connections are considered as hollow cylinders of 3 mm thickness to simplify their implementation. They should be U-shaped from one slot to another but it is sufficient to consider an equivalent hollow cylinder, attached to the windings in the slots, and having same mass. A machine

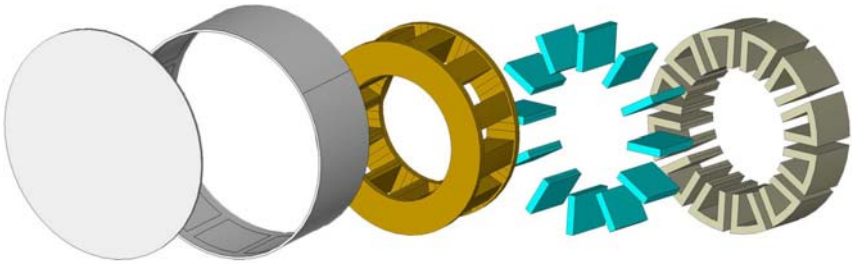

Figure 8. Exploded view of the machine modeled with commercial FEA software. From left to right: End-bells, frame, windings with end-connections, permanent magnets and U-core laminations.

having 12 slots is modeled with commercial FEA software (ANSYS) and an exploded view is presented in Fig. 8.

4.5. Natural Frequencies

The input current interacts with the magnetic field. This interaction results in high-frequency forces acting on the inner stator core surface. These electromagnetic forces excite the whole stator in the corresponding frequency range. It then leads to mechanical vibrations and noise. As a matter of fact, the stator yoke surface vibrates at frequencies corresponding to the electromagnetic forces frequencies. The air surrounding the machine is also excited to vibrate, leading to acoustic noise.

A pulsating force component of a given frequency of pulsation will produce sinusoidal deformations in the stator and rotor along the circumference. These radial forces are generally expressed as waves along the air gap. The meaning of a force-wave depends on its magnitude, frequency and the mode of excitation associated with it. The excitation force being oscillatory, the system has to respond at the frequency of excitation. Resonance occurs when this frequency coincides with one of the natural frequencies. At resonance, the distribution of vibration displacements follows sinusoidal patterns around the circumference (circumferential modes of vibrations) and the axial length of the machine (longitudinal modes of vibrations). In particular, the number of cycles of deformation around the circumference of the stator defines the number of the circumferential mode.

The basic equation for the dynamic behavior of a structure can be expressed by (10) [40]:

$$[M]\{\ddot{U}\} + [C]\{\dot{U}\} + [K]\{U\} = \{F(t)\} \tag{10}$$

$[M]$ is the total mass matrix of the structure, $[C]$ is the structural damping matrix, $[K]$ is the stiffness matrix, $\{F(t)\}$ is the vector of applied forces and $\{\ddot{U}\}$, $\{\dot{U}\}$, $\{U\}$ are respectively nodal accelerations, velocities and displacements vectors. Natural frequencies of the stator/frame assembly are obtained thanks to a 3-D modal FEA. Modal analysis is a dynamic analysis concerned with the prediction of the natural frequencies and mode shape of undamped structures under free vibrations [40]. As a result, the governing Equation (10) becomes the eigenvalue problem (11), considering a sinusoidal vibration.

$$\left([K] - \omega^2 [M]\right)\{U\} = 0 \tag{11}$$

Solving the last equation gives natural frequencies with associated circumferential and axial mode shapes. Only circumferential modes are reported in this study. In fact, on the one hand, the frame is clamped at both ends but zero axial mode orders appear on the stator yoke since its ends are free. On the other hand, as the electromagnetic force has been computed in 2-D, a constant pressure along the axial length is considered, which leads to zero axial mode orders. Stator deformations for pure circumferential modes, m, 2 and 3 are shown in Fig. 9. First natural frequencies are given in Table 4. Thus, only circumferential modes smaller or equal to 5 are of interest.

Harmonic content of the normal electromagnetic force under operating conditions presented in Fig. 6 show large differences in amplitudes for the five first harmonics depending on configurations. Amplitude of the electromagnetic pressure DC component increases with the number of rotor poles. Thus, this component should contribute to noise generation increasingly with rotor poles number around

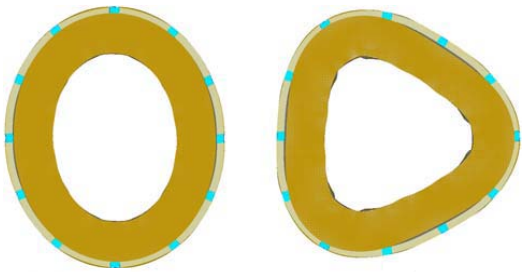

Figure 9. Displaced structure due to pure circumferential modes: (a) 2 and (b) 3.

Table 4. Natural frequencies of the stator/frame assembly.

Pure circumferential mode	Frequency (Hz)
0	11490
1	16890
2	3414
3	8185
4	13360
5	18420
(6)	(20501 >20000)

11490 Hz. The natural frequency of 11490 Hz is associated with circumferential mode 0 due the shape of the deformation. This mode is sometimes called the "breathing" mode since the deformation is uniformly distributed around the stator circumference. Though, it does change periodically with time. A distinction has to be made between space and time harmonics. Resonance occurs when there is a spatial coincidence between electromagnetic force harmonics of a given order and an associated circumferential mode number and when there is a temporal coincidence between electromagnetic force frequencies and natural frequencies.

The second magnetic force spatial harmonic of each of 12s11rp and 12s13rp configurations is almost the same and should show much larger contribution to noise generation than the second harmonic of the 12s{10,14}rp cases. Contribution of the third and fifth harmonics should appear at 8185 Hz and 18420 Hz solely for 12s{11,13}rp configurations.

The influence of magnets has been plotted in Fig. 10 for circumferential modes 0 and 2 with longitudinal modes, n, 0 and 1. Circumferential modes above 2 show the same tendency than mode 2 and do not need to be plotted. These results were achieved with FEM models and the contact between magnets and core is supposed to be perfect. A frame and stator assembly without magnets has a core made of complete steel sheets and thus exhibits much lower natural frequencies than a stator made of several cores. Starting from ratio of magnet width to magnet-plus-teeth width of 20% as illustrated in Fig. 11, a further increase in the part of magnets compared to steel in teeth leads to a slight decrease in frequencies associated with circumferential modes 0 and any longitudinal mode. For circumferential modes greater than or equal to 2, a similar decrease with a gentler slope is sighted for longitudinal mode 0. However, for non-zero longitudinal modes, a significant increase of 150 Hz every 10% increased part of magnet compared to steel can be noticed. This is also observed for every other longitudinal mode. As a conclusion, one can remark that the presence of magnets increases any natural frequency and the larger the magnets, the higher is the frequency of longitudinal modes greater than 0, except for circumferential mode 0.

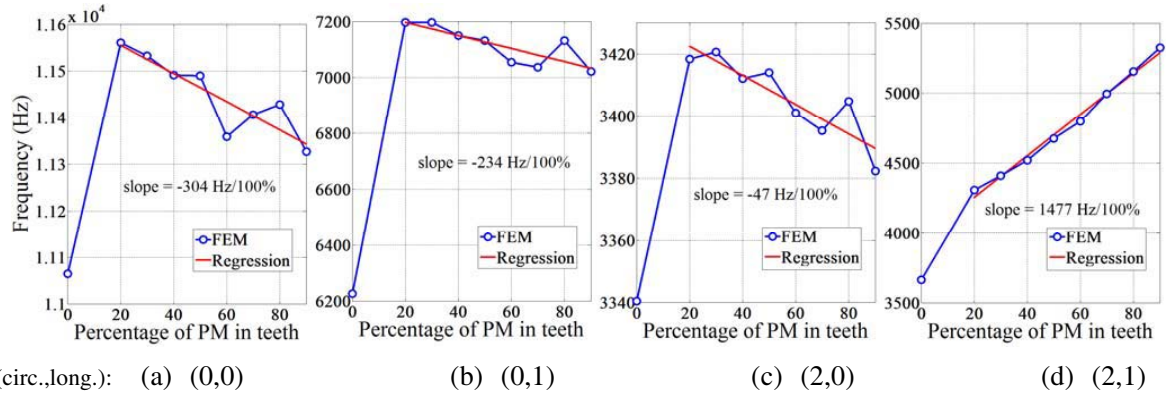

Figure 10. Natural frequencies change due to permanent magnets thickness in the machine.

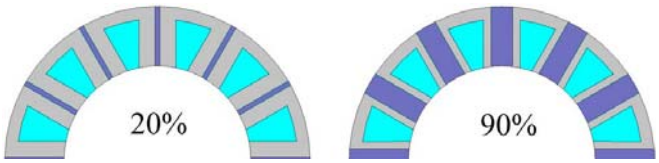

Figure 11. Illustration of ratio of magnet width to magnet-plus-teeth width.

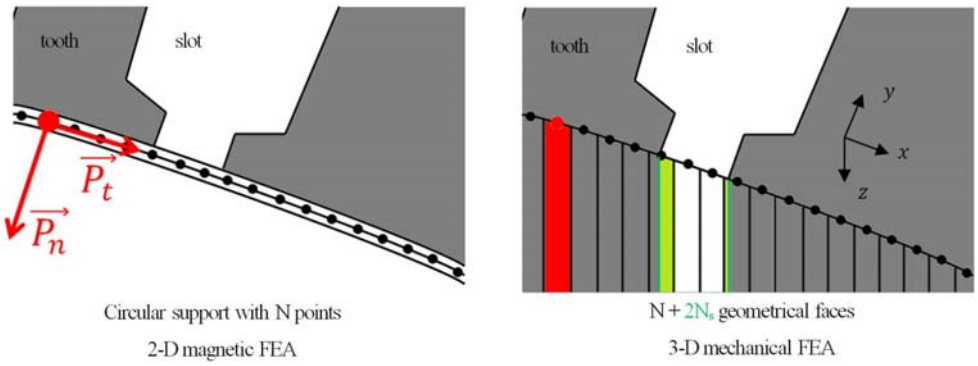

Figure 12. Distribution of magnetic force on mechanical nodes.

4.6. Noise Generation

This paper shows a case of multiphysics computation which major difficulty lies in the coupling between the magnetic model giving the electromagnetic force distributions at the stator inner surface, and the mechanical model for vibration calculations. In the 2-D electromagnetic model, the magnetic force is calculated on a circular path which has N uniformly distributed points. These points are located in the air gap close to the stator inner surface and are independent of the mesh as shown in Fig. 12. In the mechanical model, the inner stator surface is divided into N identical faces corresponding to the points of the previously created path in the electromagnetic model. Magnetic pressure is then applied on faces belonging to the teeth, at the inner radius, and subsequently to the nodes belonging to these faces. As a result, electromagnetic pressure is considered constant over the machine's axial length. N is a multiple of N_s (for symmetrical reasons) chosen in such a manner that the harmonic content of the N-sampled magnetic force curve is close to the one issued from the 2-D electromagnetic model. Here, the number of areas is chosen equal to 5 per slot angle, which is in total 240.

Sound power level spectra are computed using a 3-D harmonic FEA. This type of analysis is used to determine the steady-state response of a structure to loads that sinusoidally vary with time. Sound

originates from vibrations that are affected by the mechanical damping in the structure [19]. Damping is strongly impacted by windings and laminations making its value impossible to obtain analytically. The empirical formula (12) is instead used [41]. It relates the damping d with frequency f.

$$d(f) = \frac{1}{2\pi}\left(2.76 \times 10^{-5} f + 0.062\right) \tag{12}$$

The above characterization does not depend on mode number. However, it has been shown in [42] that damping varies with mode numbers. For the machine studied in [42], damping values have been plotted in Fig. 13 and compared to the ones calculated by (12) [41]. Damping is not linear. However, another curve, where only pure circumferential modes are joined, has been added. It is almost linear for pure circumferential modes and as only these modes are studied in the present paper, (12) is a sufficient approximation.

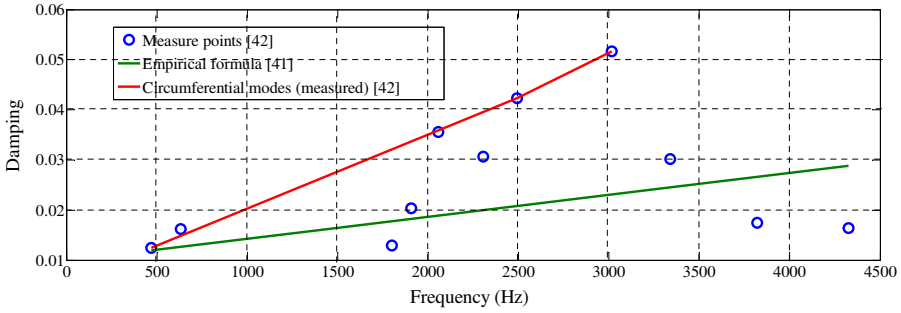

Figure 13. Damping versus frequency from empirical formula (12) [41] and experiment measurements [42].

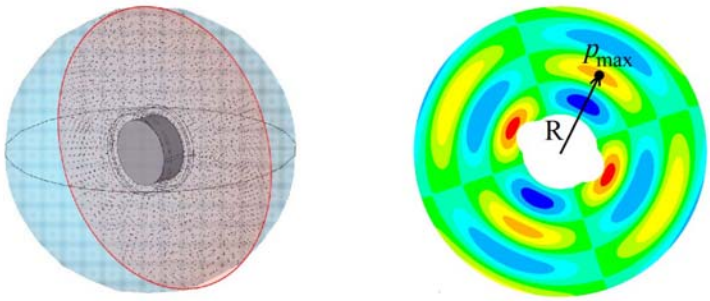

Figure 14. Cross-section to obtain acoustic power: (a) Nodes located on the cross-section, (b) local extrema and corresponding notations for circumferential mode 2.

Acoustic pressure in the air surrounding the machine is calculated every 40 Hz, on a cross-section. This section is located at the middle of the machine's axial length as shown in Fig. 14(a). At each node of this section, acoustic pressure is computed, and can be plotted, as in Fig. 14(b) for pure circumferential mode 2. Sound wave is a damped sine wave and white dots represent the location of local pressure extrema. From an extremum $p_{\max}$ located at radius R, sound power level L_W can be calculated by (13).

$$L_w = 20\log_{10}\left(\frac{p_{\max}}{\sqrt{2}p_{ref}}\right) + 10\log_{10}\left(S_{\text{sphere}}\right) \tag{13}$$

The normalized reference pressure corresponding to 0 dB, p_{ref}, is equal to 2×10^{-5} Pa. S_{sphere} is the surface of the sphere of radius R, depicted in Fig. 14(b). Sound power level of the 12s13rp configuration is taken as an example in Fig. 15. The pressure exerted on the stator inner surface is the

total electromagnetic pressure against angular position in mechanical degrees shown in Fig. 6(c). On the same plot, modal analysis is performed. Sound power level is simulated for each pressure harmonic solely (rank 0 to 5). Noting $P_n^{(i)}$ the normal pressure harmonic amplitude of rank i, and θ_s the angular position in the stator frame, pressure applied in each simulation corresponds to a sine wave given by (14).

$$P_n(\theta_s) = P_n^{(i)} \cos(i\theta_s) \tag{14}$$

Contribution of harmonic rank 0 is prevailing over every other harmonics for frequencies greater than 6 kHz. Harmonic rank 2 is practically the sole harmonic present for [0 Hz; 6 kHz] range. As a result, only small influence of pressure harmonics can be observed at frequencies corresponding to modes 1, 3, 4 and 5. Due to the stator shape of electric machines, mode 2 seems to be the most encountered first observable mode [4, 7, 17–24, 26, 27, 31, 42, 43]. Thus, as damping increases with frequency, this mode is the less damped. Also, in FSPM machines, the most excited pressure harmonics are of orders kN_r, $k \in \mathbb{N}$, which in the hearing range results in the sole excitation of mode 0, for proposed configurations. This mode is related to the attraction of the stator by the rotor. For these reasons, pure circumferential modes 0 and 2 have the strongest impact on noise generation.

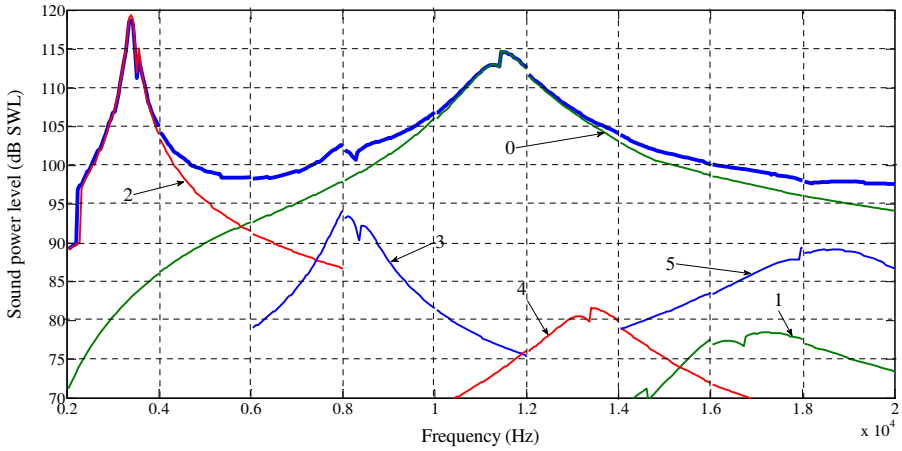

Figure 15. Contribution of single pressure harmonics to the total sound power level of the 12s13rp configuration.

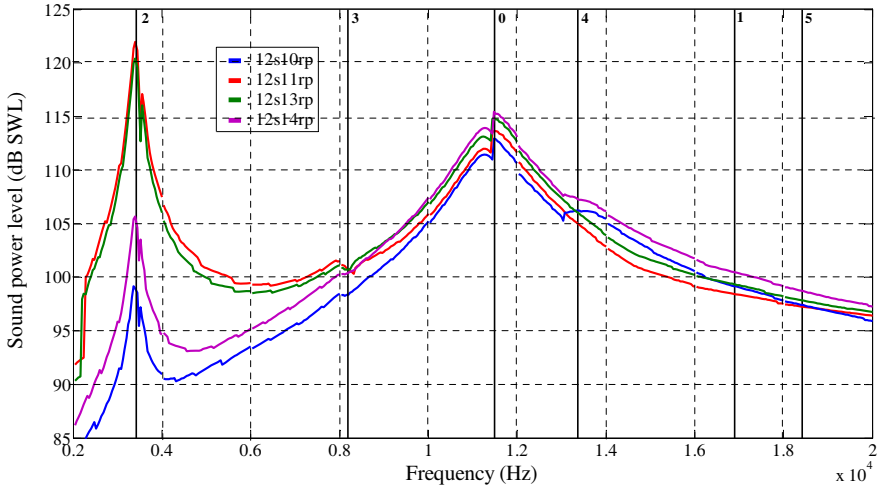

Figure 16. Sound power levels of the four configurations in the range [2 kHz; 20 kHz] with corresponding pure circumferential modes.

Table 5. Impact of harmonics of pressure on sound pressure levels for every investigated configuration. (blue line = pressure, red line = SWL).

Mode	Rotor poles	10	11	13	14	Graphical comparison
0	Harmonic of P_n (Pa)	2.40×10^5 Ref.	2.70×10^5 +13%	3.06×10^5 +28%	3.29×10^5 +37%	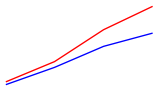
	SWL (dB)	112.9 Ref.	113.6 +0.6%	114.7 +1.6%	115.5 +2.3%	
1	Harmonic of P_n (Pa)	-	1.25×10^4	6.40×10^3	-	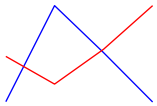
	SWL (dB)	99.18	98.46	99.36	100.5	
2	Harmonic of P_n (Pa)	9.31×10^3 Ref.	1.12×10^5 +1103%	9.68×10^4 +940%	1.20×10^3 −87%	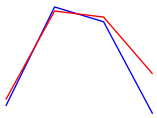
	SWL (dB)	98.97 Ref.	122.0 +23%	120.4 +22%	105.7 +6.8%	
3	Harmonic of P_n (Pa)	-	9.64×10^3	9.15×10^3	-	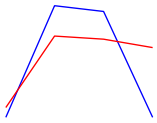
	SWL (dB)	98.33	100.8	100.7	100.4	
4	Harmonic of P_n (Pa)	1.03×10^5 Ref.	3.96×10^3 −96%	1.52×10^3 −99%	8.82×10^4 −14%	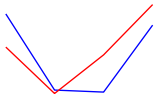
	SWL (dB)	106.2 Ref.	105.0 −1.1%	106.0 −0.2%	107.3 +1.0%	
5	Harmonic of P_n (Pa)	-	1.27×10^3	3.41×10^3	-	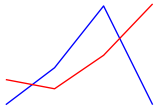
	SWL (dB)	97.43	97.27	97.85	98.74	

Sound power levels of the four investigated configurations are shown in Fig. 16 in the range [2 kHz; 20 kHz]. Also, Table 5 is provided where amplitudes of pressure harmonics from Fig. 6 and amplitudes of SWL from Fig. 16 are reported to help efficient comparison. The 12s10rp configuration serves as a basis for percentage computation. Finally, a graphical comparison is proposed showing the impact of pressure harmonics on SWL. A strong link between pressure harmonics and SWL can be observed at frequencies corresponding to modes 0 and 2 since, as shown by Fig. 15, these modes are dominant. As a result, increasing values of rank 0 pressure harmonic, as shown in Section 3, leads to increasing values of SWL, with a similar shape. Except for those two modes, there is no direct link between amplitudes of harmonics and SWL. However, they are sufficient to characterize maximum SWL and assess which configuration is the noisiest.

Maximum SWL is reached at frequencies corresponding to mode 0 for 12s{10,14}rp and to mode 2 for 12s{11,13}rp configurations. For every configuration, pressure harmonic of mode 2 has lower amplitude than one of mode 0. Though, resulting noise at the frequency corresponding to mode 2 can be higher than the one corresponding to mode 0, mode 2 appears at lower frequency and is then less damped. The 12s11rp configuration is noisier than the 12s13rp one for frequencies lower than 8 kHz (mode 3). Past this frequency, the 12s13rp is noisier than the 12s11rp and the 12s14rp is the noisiest of all. Past frequency corresponding to vibrational mode 4, the 12s11rp configuration is the less noisy one, followed by the 12s13rp one. However, they can cause translational vibration at frequency corresponding to mode 1 [43]. Though, as shown in Fig. 16, this mode has no impact on noise. Finally, on the hearing range, the 12s10rp configuration is on average the less noisy configuration.

5. CONCLUSION

A complete electro-vibro-acoustic FEA model has been described in this paper. It allows the comparison of electromagnetic noise of FSPM machines having different number of rotor poles, for nominal operating conditions. Air gap flux densities and electromagnetic pressure have been computed. It then served as a boundary condition, on the stator inner surface, to structural and acoustical models. The structural model permitted to show that the increase of the magnet width modifies the stator vibration behavior by increasing the natural frequencies. The link between pressure harmonics and sound power level has been established for dominant modes. This is the case of modes 0 and 2, each of them acting on different frequency range.

For any combinations, it has been shown that the contribution to noise from rank 0 pressure harmonic will increase with the rotor pole number N_r. Configurations resulting in low noise are the ones where low rank force harmonics are weaker such as $\mathrm{GCD}\,(N_s, N_r) = 2$. Configurations with $\mathrm{GCD}\,(N_s, N_r) = 1$ prove to be noisy and should be avoided due to the unbalanced magnetic force. On average on the hearing range, the 12s10rp configuration radiates less noise than the others. The effect of longitudinal modes greater than 0 could be investigated thanks to a 3-D electromagnetic FEA that would serve as input to the developed 3-D vibro-acoustic model. Also, further improvements would be a strong coupling between magnetic and mechanical computations.

REFERENCES

1. Chen, J. T. and Z. Q. Zhu, "Winding configurations and optimal stator and rotor pole combination of flux-switching PM brushless AC machines," *IEEE Trans. Energy Conversion*, Vol. 25, No. 2, 293–302, 2010.
2. Rauch, S. E. and L. J. Johnson, "Design principles of flux-switching alternators," *AIEE Trans. Power Apparatus and Systems*, Vol. 74, No. 3, 1261–1268, 1955.
3. Hoang, E., A. H. Ben-Ahmed, and J. Lucidarme, "Switching flux PM polyphased synchronous machines," *Proc. 7th European Conference on Power Electronics*, Vol. 3, 903–908, 1997.
4. Boisson, J., F. Louf, J. Ojeda, X. Mininger, and M. Gabsi, "Magnetic forces and vibrational behavior analysis for flux switching permanent magnet machines," *Proc. 20th International Conference on Electrical Machines*, 2988–2993, 2012.
5. Shen, J.-X. and W.-Z. Fei, "Permanent magnet flux switching machines — Topologies, analysis and optimization," *Proc. fourth International Conference on Power Engineering, Energy and Electrical Drives*, 352–366, 2013.
6. Ilhan, E., M. F. J. Kremers, E. T. Motoasca, J. J. H. Paulides, and E. A. Lomonova, "Sensitivity analysis for phase inductances in flux-switching PM machines," *Proc. 20th International Conference on Electrical Machines*, 763–768, 2012.
7. Zhu, Z. Q., Z. P. Xia, L. J. Wu, and G. W. Jewell, "Influence of slot and pole number combination on radial force and vibration modes in fractional slot PM brushless machines having single- and double-layer windings," *Proc. Energy Conversion Congress and Exposition*, 3443–3450, 2009.
8. Zhu, Z. Q., Y. Pang, D. Howe, S. Iwasaki, R. Deodhar, and A. Pride, "Analysis of electromagnetic performance of flux-switching permanent-magnet machines by nonlinear adaptive lumped parameter magnetic circuit model," *IEEE Trans. Magnetics*, Vol. 41, No. 11, 4277–4287, 2005.
9. Sidker, C., I. Husain, and W. Ouyang, "Cogging torque reduction in flux-switching permanent magnet machines by rotor pole shaping," *Proc. IEEE Energy Conversion Congress and Exposition*, 1555–1562, 2013.
10. Zhu, Z. Q. and J. T. Chen, "Advanced flux-switching permanent magnet brushless machines," *IEEE Trans. Magnetics*, Vol. 46, No. 6, 1447–1453, 2010.
11. Hua, W., M. Cheng, Z. Q. Zhu, and D. Howe, "Analysis and optimization of back EMF waveform of a flux-switching permanent magnet motor," *IEEE Trans. Energy Conversion*, Vol. 23, No. 3, 727–733, 2008.

12. Chen, J. T. and Z. Q. Zhu, "Coil connections and winding factors in flux-switching PM brushless AC machines," *COMPEL*, Vol. 30, No. 1, 84–97, 2011.
13. Kim, D. H., D. A. Lowther, and J. K. Sykulski, "Efficient global and local force calculations based on continuum sensitivity analysis," *IEEE Trans. Magnetics*, Vol. 43, No. 4, 1177–1180, 2007.
14. Melcher, J. R., *Continuum Electromechanics*, MIT Press, 1981.
15. Kim, D. H., D. A. Lowther, and J. K. Sykulski, "Efficient force calculations based on continuum sensitivity analysis," *IEEE Transactions on Magnetics*, Vol. 41, No. 5, 1404–1407, 2005.
16. Li, M. and D. A. Lowther, "Local electromagnetic force computation in the presence of numerical field errors," *IEEE Transactions on Magnetics*, Vol. 45, No. 3, 1344–1347, 2009.
17. Wang, C., J. C. S. Lai, and D. W. J. Pulle, "Prediction of acoustic noise from variable-speed induction motors: Determinist versus statistical approaches," *IEEE Transactions on Industry Applications*, Vol. 38, No. 4, 1037–1044, 2002.
18. Wang, C. and J. C. S. Lai, "Vibration analysis of an induction motor," *Journal of Sound and Vibration*, Vol. 224, No. 4, 733–756, 1999.
19. Gieras, J. F., C. Wang, and J. C. S. Lai, *Noise of Polyphase Electric Motors*, CRC Press, 2005.
20. Watanabe, S., S. Kenjo, K. Ide, F. Sato, and M. Yamamoto, "Natural frequencies and vibration behaviour of motor stators," *IEEE Transactions on Power Apparatus and Systems*, Vol. 102, No. 4, 949–956, 1983.
21. Singal, R. K., K. Williams, and S. P. Verma, "Theoretical and experimental study of vibrational behaviour of laminated stators of electrical machines," *Mechanical Systems and Signal Processing*, Vol. 6, No. 6, 535–549, 1992.
22. Torregrossa, D., F. Peyraut, B. Fahimi, J. M'Boua, and A. Miraoui, "Multiphysics finite-element modeling for vibration and acoustic analysis of permanent magnet synchronous machine," *IEEE Transactions on Energy Conversion*, Vol. 26, No. 2, 490–500, 2011.
23. Girgis, R. S. and S. P. Verma, "Resonant frequencies and vibration behaviour of stators of electrical machines as affected by teeth, windings, frame and laminations," *IEEE Transactions on Power Apparatus and Systems*, Vol. 98, No. 4, 1446–1455, 1979.
24. Williams, K., R. K. Singal, and S. P. Verma, "Vibrations of long and short laminated stators of electrical machines. Part II: Results for long stators," *Journal of Sound and Vibration*, Vol. 129, No. 1, 15–29, 1989.
25. Zhu, Z. Q. and D. Howe, "Electromagnetic noise radiated by brushless permanent magnet DC drives," *International Conference on Electrical Machines and Drives*, 606–611, 1993.
26. Lanfranchi, V., A. Aït-Hammouda, G. Friedrich, M. Hecquet, and A. Randria, "Vibratory and acoustic behavior of induction traction motors, machine design improvement," *Industry Applications Conference*, 843–848, IAS Annual Meeting, 2006.
27. Long, S. A., Z. Q. Zhu, and D. Howe, "Vibration behaviour of stators of switched reluctance motors," *IEE Proceedings on Eletric Power Applications*, Vol. 148, No. 3, 257–264, 2001.
28. Wang, H. and K. Williams, "Effects of laminations on the vibrational behaviour of electrical machine stators," *Journal of Sound and Vibration*, Vol. 202, No. 5, 703–715, 1997.
29. Garvey, S. D., "The vibrational behaviour of laminated components in electrical machines," *International Conference on Electrical Machines and Drives*, 226–231, 1989.
30. Garvey, S. D., J. E. T. Penny, M. I. Friswell, and A. W. Lees, "The stiffening effect of laminated rotor cores on flexible-rotor electrical machines," *International Conference on Vibrations in Rotating Machinery*, 193–202, 2004.
31. Verma, S. P. and A. Balan, "Determination of radial-forces in relation to noise and vibration problems of squirrel-cage induction motors," *IEEE Transactions on Energy Conversion*, Vol. 9, No. 2, 404–412, 1994.
32. Anonymous, "Non oriented electrical steel — Typical data," SurahammarsBruk, Cogent, Tata Steel, 2014.
33. Bouzek, L. and R. Pechanek, "Vibration behaviour of the asynchronous machine magnetic core," *European Conference on Power Electronics and Applications*, 1–7, 2013.

34. Borisavljević, A., "Limits, modeling and design of high-speed permanent magnet machines," Springer Theses, Recognizing Outstanding Ph. D. Research, Springer-Verlag, 2013.
35. Niu, M. C. Y., *Composite Airframe Structures*, 3rd Edition, Hong Kong Conmilit Press Limited, 2010.
36. Ting, T. C. T. and T. Chen, "Poisson's ratio for anisotropic elastic materials can have no bounds," *The Quarterly Journal of Mechanics and Applied Mathematics*, Vol. 58, No. 1, 73–82, 2005.
37. Reinhardt, F. and H. Soeder, "Atlas des mathématiques," La Pochothèque, Encyclopédies d'Aujourd'hui, Librairie Générale Française, 1997.
38. Tang, Z., P. Pillay, A. M. Omekanda, C. Li, and C. Cetinkaya, "Young's modulus for laminated machine structures with particular reference to switched reluctance motors vibrations," *IEEE Transactions on Industry Applications*, Vol. 40, No. 3, 748–754, 2004.
39. Wang, C., J. C. Lai, and A. Astfalck, "Sound power radiated from an inverter driven induction motor. Part 3: Statistical energy analysis," *IEE Proceedings on Electric Power Applications*, Vol. 152, No. 3, 619–626, 2005.
40. Fagan, M. J., *Finite Element Analysis: Theory and Practice*, Longman Scientific & Technical, 1992.
41. Yang, S. J., *Low-noise Electrical Motors*, Clarendon Press, 1981.
42. Balan, A., "Theoretical and experimental investigations on radial electromagnetic forces in relation to vibration problems of induction machines," Ph.D. dissertation of Saskatoon University, 1997.
43. Huo, M., S. Wang, J. Xiu, and S. Cao, "Effect of magnet/slot combination on triple-frequency magnetic force and vibration of permanent magnet motors," *Journal of Sound and Vibration*, Vol. 332, 5965–5980, 2013.